ORIGINAL ARTICLE

Service-Life Damage Assessment of a Reinforced Concrete Structure under Multi-Hazard Seismic and Wind Actions

Pratik Bhaskar[1] · Akshay Baheti[1] · Vasant Matsagar[1]

Abstract

Service-life damage in reinforced concrete (RC) structure caused due to the actions of earthquake and cyclonic wind, and their multi-hazard effects is evaluated, by considering them as independent (uncorrelated) non-cascading hazards with and without considering the effects of chloride-induced corrosion in the structural members. Behavior of a structure to a certain hazard during its service life is affected by some past damages induced therein, albeit minor sometimes, and which are not often considered in the design process of the structure. In this study, a rectangular-plan 9-storey RC special moment-resisting frame (SMRF) building, assumed to be located in a region which is prone to both, seismic and wind activities, has been designed for various conventional load combinations prescribed by the relevant Indian standards/ design codes. The structural damage is evaluated in terms of a damage index, by performing nonlinear dynamic analysis for site-specific spectrum-compatible earthquake and local cyclonic wind conditions, while considering their cumulative effect on the structure as non-cascading independent hazards. Also, updated factor of safety for the column base has been determined after the building is exposed to different possible hazard scenarios. It has been observed that the damage in the RC structure due to independent earthquake and wind events can increase from 10% to even 200% when the effect due to chloride-induced corrosion in the structural members is considered in the analysis. Also, multi-hazard actions on the structure results in 1.5-fold increased damage as compared to the damage induced due to individual hazards, when the effect of corrosion of steel reinforcement is considered. Hence, a more realistic, rational, and holistic life cycle-based design approach has been presented here, based on the actual behavior of the structure that needs to be adopted while practicing design of structures under multiple hazards.

Introduction

Structures are being designed for the broad range of static and dynamic loads, arising due to natural and anthropogenic activities, so that it would not fail or collapse, for the purpose of saving lives rather than mere preservation of the structure itself. This approach is fundamentally adopted in structural engineering profession for design of structures. In India, design of a reinforced concrete (RC) structures is governed by the most severe (worst) possible loading scenario on the structure, which is determined through various load combinations given in the Indian standard, IS 456 (BIS 2000). However, this approach may sometimes result in uneconomical and unconservative design of a structure (Nikellis et al. 2019), as a typical structure is subjected to multiple natural hazards of varying intensity, during its service-life or lifetime. Roy and Matsagar (2021a) presented a world map with different zones under the actions of several natural hazards. As per the data, approximately 3.5 million km^2 area in the world is exposed to two or more natural hazards during service-life of a structure. Also, frequency of these hazardous incidences has tripled over the last three decades (Chen et al. 2010). Duthinh and Simiu (2010) argued that

✉ Vasant Matsagar
  matsagar@civil.iitd.ac.in

  Pratik Bhaskar
  pratik9460@gmail.com

  Akshay Baheti
  as.baheti11@gmail.com

[1] Multi-Hazard Protective Structures (MHPS) Laboratory, Department of Civil Engineering, Indian Institute of Technology (IIT) Delhi, Hauz Khas, New Delhi 110 016, India

risk of exceeding a limit state associated with multiple hazards could be twice as high as the risk associated with only one hazard. These crucial observations affect not only the safety but also the cost of construction and insurance of the structure or reinsurance companies. An optimum design should therefore ideally be derived through a service-life cost analysis that relates the performance of any structure during its lifetime with probable losses due to various loading conditions.

Multiple hazards can be classified as concurrent (e.g., wind and surge, or rainstorm and flood), cascading (e.g., fire following earthquake, or tsunami following earthquake), and independent hazards or hazards that are likely to occur at different times (e.g., wind and earthquake) (Gardoni and LaFave 2016). Out of these, mutually non-cascading and independent hazard events pose a significant threat to the civil infrastructures (Aly and Abburu 2015) as the effects of single hazard of medium intensity may not be sufficient due to which it may go unnoticed; however, effect of such multiple hazards may result in non-proportionate response of structures.

In this context of designing built-infrastructure under multiple hazards, some regions have been identified within India where, there is a high probability of a structure being subjected to independent action of both, strong wind forces as well as strong seismic ground motion. Considering the importance of multi-hazard effects, it is imperative to conduct systematic multi-hazard analysis of structures at these locations (Roy and Matsagar 2021b). Extensive research has been carried out on multi-hazard seismic and wind analysis of structures considering different approaches (Li and Lindt 2012; Kameshwar and Padgett 2014; Chulahwat and Mahmoud 2017; Venanzi et al. 2018; Nikellis et al. 2019; Roy and Matsagar 2019, 2020; Wang et al. 2020). Many of these cited studies have shed light on the damage caused by either multiple earthquake hazards only, or even combined influence of the earthquake and wind hazards on the structure; however, effects of corrosion-induced structural deterioration on probable response of the structure towards earthquake and wind are seldom considered which would result in holistic and more accurate multi-hazard analysis of the structure. In life-cycle assessment of a structure at risk from multiple hazards, actual health of the structure at the instant of evaluation is required to be taken into account. In addition, in all these studies, effects of structural repair and restoration processes, undertaken after the occurrence of a hazard, have not been considered on the response of the structures to probable future hazards.

The need to incorporate structural deterioration in the service-life assessment of a structure and evaluating its response under multiple hazards has emerged upon review of the past literature. In view of this, the main goal of this study is to advocate mitigation of the impact of natural hazards on an RC structure by analyzing the damages induced in the structure under multi-hazard loading scenarios and subjected to continuous chloride-induced corrosion throughout the age of the structure. Hence, the objectives of the present study are: (1) to assess service-life response of a reinforced concrete (RC) structure when subjected to non-cascading independent multiple hazards such as earthquake and wind, with and without considering the effects of corrosion-induced structural damage; and (2) to assess effects of repair, rehabilitation and/or restoration processes which are undertaken after the occurrence of a hazard on the service-life response of the structure to some future probable hazard.

The present study is aimed to analyze the impact of continuous chloride-induced corrosion in structural members on the damage caused due to site-specific earthquake and local cyclonic wind. While evaluating continuous material deterioration on account of chloride-induced corrosion in the RC structure, effect of periodic structural maintenance in terms of decrease in the rate of corrosion is not considered to capture worst possible structural response under earthquake or wind excitation. A good volume of literature deals with the effects of rate of corrosion on the deterioration of structural members.

Incidence time of both the hazards, earthquake and wind, is kept as variable during the intended service-life of the structure, i.e., design life of 100 years. The impact of the multi-hazard effects on the structure is compared with the individual action of each hazard in the presence and absence of the chloride-induced corrosion in structural members considering effects of repair, rehabilitation and/or restoration processes after occurrence of the hazard occurred a priori. This impact is measured in terms of cumulative damage index and residual axial load-carrying capacity of the column base to determine the change in the available factor of safety (FOS) during the service-life of a structure.

Numerical Modeling

In the present study, the structure is considered located in Bhuj (Kachchh district of Gujarat in India), which is prone to both regular earthquake and high-speed wind hazards, as given in relevant Indian standards. This region is listed in Annex P of National Building Code (NBC) of India (BIS 2016b) for being exposed to greater risk of multi-hazard effects from both, earthquake and wind. Furthermore, the presence of sea nearby severely influences chloride-induced corrosion in structural members having steel utilized in the construction. Herein, the role played by the chloride current is shown by comparative analysis of the damage inflicted in the structure under the actions of site-specific earthquake and local cyclonic wind. The loads calculated for the

example structure studied here pertain to the conditions prevail at site located in Bhuj.

Structural Modeling

As the study focuses on a structure exposed to both earthquake and cyclonic wind hazards, height of the building is chosen so as to capture the considerable influence from both the types of hazards in low to medium-rise structures. As per the Indian standard, IS 875 (BIS 2015), for a structure having fundamental frequency less than 1 Hz or a structure with overall aspect ratio 5 or more is to be designed with the inclusion of a gust factor in the wind loading. Height of the building is kept at 31.5 m considering 9-storey structure with floor-to-floor height of 3.5 m, as shown in Fig. 1a. The 9-storey building is assumed to be having uniform floor plan at each floor. The plan dimension is assumed as 12 m × 9 m with uniform bay width of 3 m, as shown in Fig. 1b. Beam element is placed at boundary of each bay to support the masonry wall of thickness 0.23 m. Since the objective of the present study is to devise a generic methodology for performing holistic multi-hazard analysis of the structure, for simplicity and maintaining symmetry in the structure, uniform column and beam dimensions of 0.6 m × 0.6 m and 0.25 m × 0.5 m, respectively are adopted in the structure, which are rather overdesigned, i.e., conservative design

with higher factors of safety (FOS). Grade of concrete and steel reinforcement bars used for design of the structure are M30 (characteristic compressive strength, $f_{ck} = 30$ MPa) and Fe415 (characteristic yield strength, $f_y = 415$ MPa), respectively. Table 1 provides some details of the loads considered to be acting on the structure as per the relevant Indian standards mentioned there. The structure is then analyzed for different load combinations as enlisted in the IS 456 (BIS 2000). Clear cover of 15 mm, 25 mm, and 40 mm thicknesses is provided to the main steel reinforcement bars in slab, beam, and column, respectively assuming that the structural elements are subjected to severe exposure, as defined in the IS 456 (BIS 2000). Steel reinforcement areas in column elements are determined at the end of the analysis to prevent the structure from exceeding limit state in strength and serviceability under any design load combination. Thus, the RC column members are provided with 28 rebars of 12 mm diameter with the reinforcement bars uniformly distributed on each face of the square column.

The designed structure is modeled as a three-dimensional (3D) space frame with its structural members modeled as linear 2-node beam-column elements. Fixed boundary condition is applied at the base of each column. The resultant structure is idealized in mass matrix, M and stiffness matrix, K as given in Eqs. (1) and (2), respectively. The self-weight of the structure, superimposed dead load on

Fig. 1 **a** Elevation; **b** floor plan; **c** quasi-static pushover curve for a selected hinge on the roof in undamaged state; and **d** peak top floor response of the 9-storey RC structure
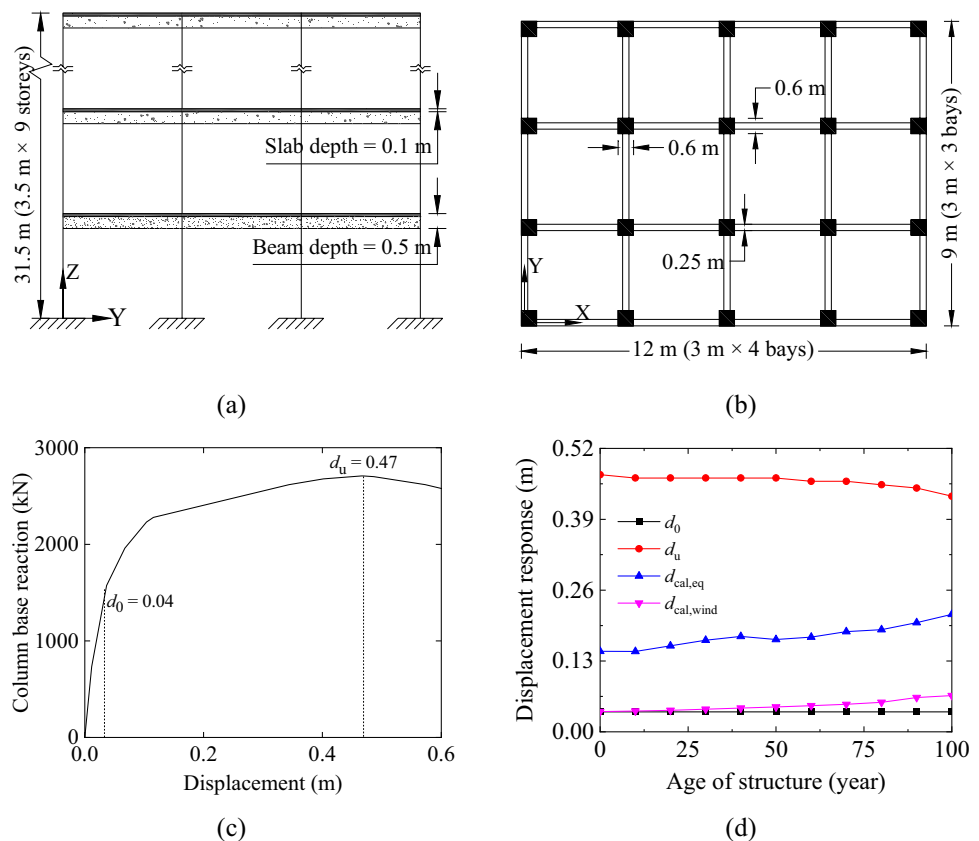

(a)

(b)

(c)

(d)

Table 1 Summary of loading on the 9-storey RC special moment-resisting frame (SMRF) building under study

Sl No	Load Pattern	Load case
1	Dead load (BIS 1987a)	(a) Self-weight of frame (Concrete density = 25 kN/m^3)
		(b) 14 kN/m wall load on the beams of each non-roof floors
		(c) 2.5 kN/m^2 slab loads on each floor
		(d) 1 kN/m^2 superimposed dead load
2	Live load (BIS 1987b)	(a) 2.5 kN/m^2 on each non-roof floors
		(b) 0.75 kN/m^2 on roof
3	Earthquake load (BIS 2016a)	Zone V (location—Bhuj); Importance factor, $I = 1$; Response reduction factor, $R = 5$; medium soil strata
		Mass source = Dead Load + 0.25 × Live Load
4	Wind load (BIS 2015)	Basic wind velocity = 50 m/s; Risk coefficient, $k_1 = 1.08$; Terrain roughness and height factor, $k_2 = 1.065$; Topography factor, $k_3 = 1.0$; Importance factor for cyclonic region, $k_4 = 1.0$

structural members, and 25% of the live load contributed to the mass lumped at each node in this numerical model. Since beam-column joints are assumed rigid, stiffness of each column is evaluated considering fixed–fixed condition at both of its ends.

$$M = \begin{bmatrix} m_1 & 0 & 0 & \cdots & 0 \\ 0 & m_2 & 0 & \cdots & 0 \\ 0 & 0 & m_3 & \cdots & 0 \\ \vdots & \vdots & \vdots & \ddots & \vdots \\ 0 & 0 & 0 & \cdots & m_n \end{bmatrix} \tag{1}$$

$$K = \begin{bmatrix} k_1 + k_2 & -k_2 & 0 & \cdots & 0 \\ -k_2 & k_2 + k_3 & -k_3 & \cdots & 0 \\ 0 & -k_3 & k_3 + k_4 & \cdots & 0 \\ \vdots & \vdots & \vdots & \ddots & \vdots \\ 0 & 0 & 0 & \cdots & k_n \end{bmatrix}, \tag{2}$$

where n is the number of nodes in the structure; m_* and k_* respectively denote nodal lumped mass and stiffness of the beam elements used in the numerical modeling. Structural damping matrix is evaluated using the classical Rayleigh damping relation (Chopra 2016) for mass and stiffness proportional damping as given in Eq. (3), as:

$$C = a_0 M + a_1 K \tag{3}$$

in which, coefficients for mass (a_0) and stiffness (a_1) are derived using relations given in Eqs. (4) and (5), respectively as:

$$a_0 = \frac{2\xi \omega_1 \omega_c}{\omega_1 + \omega_c} \tag{4}$$

$$a_1 = \frac{2\xi}{\omega_1 + \omega_c}, \tag{5}$$

where ξ is the damping ratio, assumed 5% for the reinforced concrete (RC) structure; ω_1 and ω_c correspond to natural frequencies of the structure in mode 1 and cut-off mode shape, respectively. Third mode shape is assumed to be the cut-off mode shape for calculation of these coefficients for damping.

Structural Deterioration due to Chloride-Induced Corrosion

Reinforced concrete (RC) structures suffer from continuous material degradation depending on their location, apart from several natural hazards of varying intensities experienced during the lifetime of the structures. Environmental agents lead to deterioration, imparting continuous damage to the structural elements in the form of corrosion of the steel reinforcement bars, development of cracks and their propagation, spalling of concrete, and other such distress. Corrosion of the steel reinforcement is one of the major deteriorating mechanisms in the RC structures, especially for those located nearby a water body where it may further accelerate. In such condition, the structure is continuously exposed to corrosion-inducing elements such as H_2O, O_2, Cl^-, and CO_2. The penetration of corrosive elements toward the reinforcement placed within concrete depends on the permeability and the finishing of the concrete surface, and once there is enough accumulation of these elements around the reinforcement, process of corrosion is initiated and almost constantly progresses. Steel material from the reinforcement bars (rebar) is consumed in the process of corrosion and rust starts forming around the rebar. Due to the rust formation, effective diameter of reinforcement reduces. As the rust volume is higher compared to the loss of rebar area due to corrosion, pressure builds up on the surrounding concrete. This results in increase in the overall volume of the reinforcement, which leads to stress initiation in the surrounding region of concrete. Finally, cracks appear in concrete, which further opens the path for corrosion by allowing faster propagation of these elements to the reinforcement through the newly opened cracks (Zhou et al. 2015). Chloride-induced corrosion is hence a continuous

process and causes widespread damage to the RC structure, resulting significant reduction in the service-life of the structure (Basheer et al. 1996). The effects of chloride-induced corrosion in the structure have been widely studied by various researchers (Chen and Mahadevan 2008; Pack et al. 2010; Otieno et al. 2016a, b; Cui et al. 2019). The process of determining corrosion-induced damage in structures is explained in Eqs. (6)–(16). The rusted volume of steel per unit length (cm^2) is predicted as:

$$A_{st}(t) = \frac{M_{st}(t)}{\rho_{st}} = 3.709 \times 10^{-5} i_c \pi d^r(t) \Delta t, \tag{6}$$

where the density of steel (ρ_{st}) is considered 7.8 g/cm^3 and $M_{st}(t)$ is the mass loss of steel per unit length (g/cm) which is determined using the Faraday's Law given in Eq. (7) as:

$$M_{st}(t) = \frac{m_s It}{zF}, \tag{7}$$

where m_s is the atomic mass of iron (56 g for Fe); I denotes the chloride current (A), which can be expressed as the product of surface area of the steel bar (a_s) and the corrosion current density (i_c), for unit length of a rebar of diameter, d, $a_s = \pi d$. Further, t is the time after corrosion initiation (in s); z is the ionic charge (considered 2 for Fe^{2+}); and F is the Faraday's constant, i.e., 96,500 A.s (cf. Cui et al. 2019). After corrosion, the volume of rust generated can be assumed equivalent to the loss of material from the rebar. Therefore, the remaining diameter of the rebar after Δt time is determined as given in Eq. (8).

$$d^r(t) = \sqrt{d^2 - \frac{4A_{st}(t)}{\pi}}. \tag{8}$$

The chloride-induced corrosion also leads to an effective decrease in the yield and the ultimate strengths of the steel reinforcement. Residual yield and ultimate strengths of the reinforcement bar can be calculated using Eqs. (9) and (10), respectively as:

$$f_y^r = \left(1 - 0.015\eta_{100}\right)f_y^0 \tag{9}$$

$$f_u^r = \left(1 - 0.015\eta_{100}\right)f_u^0, \tag{10}$$

where f_y^r and f_u^r respectively are the residual yield and ultimate strengths of the reinforcement with respect to the f_y^0 and f_u^0 which are the yield and ultimate strengths of reinforcement bar at preliminary stage. Here, η_{100} is the percentage of steel mass lost due to the chloride-induced corrosion over the time. While there is a reduction in the yield and ultimate strengths of steel reinforcement bar, no change in the elastic modulus of steel material occurs. Hence, constant elastic modulus of 200 GPa is considered for the steel

reinforcement material. Time step (Δt) of 10 years is considered in present study to reevaluate the altered damaged state of the structure. For this purpose, a constant chloride-induced corrosion current density of 2 µA/cm^2 is assumed throughout the analysis. This data has been taken after careful consideration given to various studies including Otieno et al. (2016a) and Cui et al. (2019). The reduction in the compressive strength of concrete depends on the extent of cracks formed in the process. As per the model proposed by Vecchio and Collins (1986) given in Eq. (11), the reduced strength in concrete cover is represented as:

$$f_{ck}^* = \frac{f_{ck}}{1 + k_r \frac{\varepsilon_1}{\varepsilon_{co}}}, \tag{11}$$

where k_r is the coefficient related to bar roughness and diameter, which for medium-diameter ribbed bars is taken as 0.1 (cf. Coronelli and Gambarova 2004); ε_{co} is the strain at the peak compressive stress (f_{ck}) which is considered as 0.002 as per the guidelines given in the IS 456 (BIS 2000), and ε_1 is the tensile strain in the cracked concrete at right angles to the direction of the applied compression, evaluated by Eq. (12), as:

$$\varepsilon_1 = \frac{b_f - b_0}{b_0} \tag{12}$$

where b_0 is the section width in the undamaged state (no corrosion cracks); and b_f is the beam width increased by corrosion cracking. Using Eq. (13), an approximate increase in the beam width is calculated as:

$$b_f - b_0 = n_{bars} w_c, \tag{13}$$

where n_{bars} is the number of bars in each layer; and w_c is the crack width for a given corrosion level during the period Δt, to be evaluated using Eq. (14) as:

$$w_c = 2\pi(v_{rs} - 1)d_e, \tag{14}$$

where v_{rs} is the ratio of volumetric expansion of the oxides with respect to the undamaged material whose value is taken as 2 (cf. Molina et al. 1993); d_e is the corrosion penetration depth, which is calculated using Eq. 15 as:

$$d_e = 0.0115 \, i_{co} \, t, \tag{15}$$

where i_{co} is the corrosion current density expressed in cm/year, and t is the time after corrosion initiation (year). Further, the elastic modulus (E_c) of concrete is related with its compressive strength (f_{ck}) at each time step using the relation (Eq. 16) proposed by Noguchi and Nemati (2007) as:

$$E_c = 2.1 \times 10^5 \left(\frac{\gamma}{2.3}\right)^{1.5} \left(\frac{f_{ck}}{200}\right)^{0.5}, \tag{16}$$

where the modulus of elasticity of concrete (E_c) is expressed in kgf/cm^2, γ is density of concrete which is taken constant as 2.5 ton/m^3, and f_{ck} is the characteristic compressive strength of concrete material expressed in kgf/cm^2.

Architectural repair actions (referred as repair actions in this article) in a structure refers to modifications in a part or whole of structure to restore its appearance and service-ability. This may involve patching of defects such as cracks and fall of plaster, rebuilding non-structural walls, relaying cracked flooring at storey level, redecoration, etc (BIS 2009). There are various repair techniques available to treat the corroded concrete material such as patch repair, coating systems, electrochemical chloride extraction, etc. These techniques rely on a mechanism of removing the damaged cover concrete and replace it with fresh concrete mix. Tofeti-Lima and Ann (2020) studied the effectiveness of various electrolytes to treat concrete damaged due to chloride-induced corrosion and found that there is approximately 25% reduction in the chloride current after treating concrete with certain electrolyte. Therefore, same decrease in the chloride current density is assumed in the present study to consider the effect of structural repair on successive structural degradation caused due to chloride-induced corrosion. In addition, it is assumed that strength of concrete in cover region is restored to its original strength (at incipient stage); however, the core concrete material is not treated while performing such architectural repairs and therefore core concrete material continues to remain in the damaged state, as explained in section "Structural Damage Evaluation due to Hazards".

While architectural repair techniques are limited to treating the damaged concrete surfaces, structural repair actions (referred as the restoration process in this article) deal with restitution of the mechanical strength and thereby durability, as the building had before the occurrence of damage. It may involve cutting and rebuilding of structural elements, addition of structural materials, micro-concreting, injecting epoxy like material which possesses high tensile strength into the cracks in wall, beam, or column, etc. However, it is difficult to completely restore the structure to its original capacity (same as that in its incipient stage) and therefore in this study, it is assumed that structural restoration process restores 80% strength of all the damaged structural members without adding to its stiffness properties. This also comprises treatment of concrete surface as discussed in the architectural repair procedure and thus, restored structure results in decreased chloride current density by 25% in addition to the increase in the strength of concrete in cover and core regions. The effect of the chloride-induced corrosion on the mechanical properties of the RC structure, in the absence of repair and restoration process, for various constant chloride current densities is shown in Fig. 2a–d. It is assumed here that chloride-induced corrosion starts immediately after the structure is constructed. Variation in the fundamental

period of the structure due to such continuous degradation is presented in Fig. 3a which indicates reduced stiffness of the lateral load-resisting elements in the structure over its service-life, resulting in reduction in the fundamental frequency of the structure.

Structural Damage Evaluation due to Hazards

Damage in the structural member is a subjective term, used to relate the cracking, crushing, buckling, possible yielding of the longitudinal bars, loss of anchorage (bond failure), or alike eventualities. In general, damage in the RC member is related to irrecoverable (plastic) deformations. Quantification of such damage in the structure is possibly carried out in terms of a damage index. Various damage index models have been developed by researchers over the time based on a particular deformation quantity such as strain, curvature, nodal displacement, element forces, energy dissipated or absorbed by the structural member, etc. Reviews on such damage models have been presented by Kappos (1997), Sinha and Shiradhonkar (2012), Cao et al. (2014), Zameeruddin and Sangle (2016), Hait et al. (2019), etc. Sinha and Shiradhonkar (2012) compared damage index values resulting from some of the most popular damage models and concluded that each of the damage model results in similar values for a structure under medium intensity of dynamic loading. Therefore, among the various choices available to select from, a damage model based on displacement-ductility characteristics of a structural member, developed by Park et al. (1985) is used in the present study as per Eq. (17) to quantify the structural damage expressed as:

$$D = \frac{\left(d_{cal} - d_0\right)^{\alpha}}{\left(d_u - d_0\right)^{\alpha}},\qquad(17)$$

where d_{cal} is the peak displacement obtained by conducting nonlinear dynamic analysis of an RC structure; d_0 is a threshold value below which concrete material can be assumed to remain within elastic limit; d_u is the peak displacement after which large deformation is observed in the structure/ member, and α is an exponent which is taken as unity in the present study. The elastic displacement $\left(d_0\right)$ and ultimate displacement $\left(d_u\right)$ of the structure are obtained by performing pushover analysis of the building. The presence of masonry walls within and around the structure is neglected while performing the pushover analysis. Beams and columns are modeled as lumped plasticity elements whose force–displacement behavior is defined as per the guidelines given in FEMA 356 (2000) in absence of specific recommendations on it currently in the Indian standards. Beam and column elements are assigned nonlinear parametric M3 and P-M2-M3 plastic hinges, respectively at a distance of 0.05 times the total length of the member from

Fig. 2 Change in **a** longitudinal reinforcement bar diameter; **b** crack width; **c** compressive strength of concrete; and **d** modulus of elasticity of concrete, with corrosion current density (i_c) over the age of the structure (Cui et al. 2019)
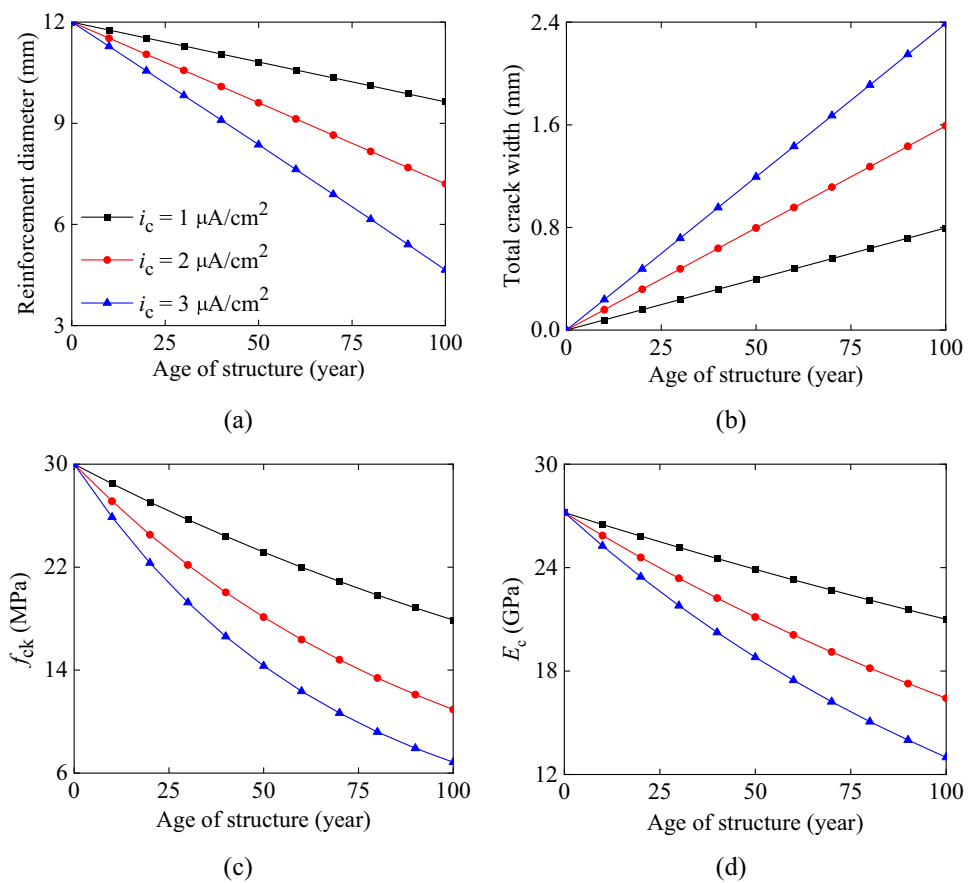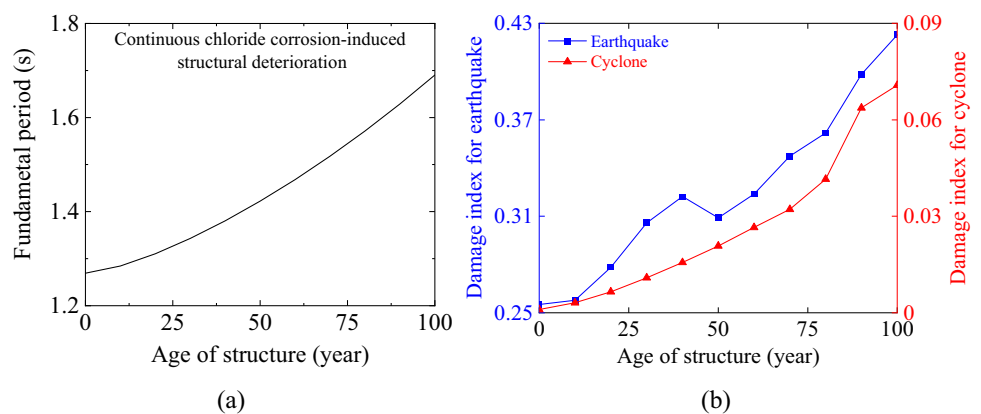

Fig. 3 **a** Change in the fundamental time period of the structure due to chloride-induced corrosion causing structural deterioration; and **b** variation in service-life damage index of the 9-storey RC structure, subjected to individual action of earthquake and cyclonic wind, for a constant corrosion current density of 2 μA/cm²

both their ends (cf. FEMA 356, 2000). Takeda model is used for concrete and kinematic hardening behavior is assumed for modeling the longitudinal steel reinforcement bars in the structural members.

The resultant pushover curve obtained through lateral displacement control analysis of the structure until the hinge yields for the 9-storey structural model of the RC building (discussed in section "Structural Modelling") is shown in Fig. 1c. For the pushover curve, a predefined hinge in a beam at the topmost floor level is monitored for the base reaction developed as the displacement is applied to it incrementally.

The same reference hinge behavior is recorded for in the single-hazard and multi-hazard analyses of the structure. The point at which the pushover curve deviates from linearity (proportionality) is identified as the elastic limit point for that reference hinge, and it is assumed that base reaction up to this loading does not result in any permanent damage caused to the structure. The corresponding value of the elastic limit displacement is taken as d_0 which is used in Eq. (17) for the calculation of the damage index. Hence, d_0, as presented in Fig. 1c for the undamaged 9-storey reinforced concrete (RC) structure under consideration is

0.04 m. The peak base reaction after which the curve starts declining is identified as the peak strength point for that beam-column element. The corresponding displacement for the peak strength point is taken as the ultimate displacement (d_u) to be used in Eq. (17) for the calculation of the damage index of the structure. As presented in Fig. 1c, the value of d_u for the undamaged 9-storey RC building is 0.47 m. Variation in the yield and ultimate points with the service-life of the structure, considering continuous deterioration caused due to chloride-induced corrosion is presented in Fig. 1d.

Damage index of a structural member represents decrease in its load-carrying capacity; therefore, there is linear correlation between damage index and reduced concrete strength (Wu et al. 2014). Furthermore, based on the principle of strain equivalence (Lemaitre 1984), linear correlation exists between strength and elastic modulus for the concrete material; thus, correlation between elastic modulus of concrete and the damage index is expressed in Eq. (18) as:

$$E_c^* = (1 - D)E_c. \tag{18}$$

It is assumed that there is no decrease in strength and elastic modulus of steel reinforcement as a result of damage in a structural member due to an incident hazard, either earthquake or wind.

Service-Life Damage Analysis of Structure under Single Hazard

Seismic Analysis of the Structure

As per the earthquake-resistant design philosophy prescribed in most of the seismic design codes worldwide, a structure is not expected to incur any damage when subjected to frequent or minor tremors (Avramidis et al. 2016). Hence, the structure is subjected to less frequent or medium intensity earthquake in this study as it may result in inducing minor damages in the structural members which may not require repair or restoration as such; thereby, they may go unnoticed unlike the case with rare (infrequent) or extreme earthquake event in which the structure undergoes large deformation and consequently mandating restoration and may be damage experienced to the extent of even possible partial or complete collapse. Due to lack of sufficient earthquake ground motion data at the site, artificial (synthetic) earthquake generation technique is suitable to evaluate response of the structure to real probable earthquake. Ferreira et al. (2020) developed an algorithm, based on the Fourier transform, to generate spectrum-compatible earthquake time-history from a given seismic ground motion. This algorithm is used to obtain an earthquake time-history compatible to the response spectrum specified in the Indian standard, IS 1893 (BIS 2016a).

So, an earthquake time-history is generated using 1999-Chamoli earthquake ground motion as a base motion, such that it is equivalent to a moderate intensity earthquake in seismic Zone V with a return period = 475 years as per IS 1893 (BIS 2016a), as presented in Fig. 4a. The corresponding response spectrum for this ground motion is presented in Fig. 4b where it is compared with the input (desirable) response spectrum as specified. Comparison of the two response spectra implies that the generated synthetic earthquake time-history represents site-specific earthquake ground motion for medium soil condition.

The 9-storey reinforced concrete (RC) structure under consideration is subjected to unidirectional excitation of the synthetic earthquake ground motion generated. Spatial variation in the ground motion is neglected as the plan area of structure is too small to observe any effects of the variability in excitation with propagation of the ground motion. Since earthquake time-history is obtained for medium soil strata as per the IS 1893 (BIS 2016a), soil-structure interaction (SSI) is also neglected in the deriving structural response. Columns at each floor are provided with diaphragm action due to the presence of the rigid RC slab. Thus, the governing differential equation of motion, Eq. (19), for the 9-storey structure, subjected to seismic excitation are written as:

$$M\ddot{x} + C\dot{x} + Kx = -M\Lambda\ddot{x}_g, \tag{19}$$

where M and K are mass and stiffness matrices of the structure as defined in Eqs. (1) and (2), respectively; C is the mass and stiffness proportional damping matrix as defined in Eq. (3); x is the relative displacement vector with respect to ground which contains floor displacement of the structure; Λ is an influence coefficient vector which contains all its elements as unity; and $\ddot{x}_g$ is the earthquake ground acceleration. Geometrical nonlinearity (P-Δ effect) is considered while performing structural analysis for seismic excitation. Newmark's average acceleration scheme (Newmark 1959) is used to evaluate the dynamic response of the structure through step-by-step integration approach. Peak top storey displacements over service-life of the structure under the action of earthquake-induced forces are presented in Fig. 1d. There is continuous increase in the peak top floor displacement as continuous structural deterioration results in increased flexible structure. The floor or storey displacements thus obtained are used to determine damage suffered by the structure using the relation given in Eq. (17). The damage index values for an earthquake hazard are evaluated for the 9-storey structure over its intended service life, i.e., 100 years while considering the continuous structural deterioration caused due to chloride-induced corrosion in all the structural members and the same is presented in Fig. 3b. There is a continuous increase in the structural damage as the structure grows old, which makes its earthquake-resistance doubtful

Fig. 4 **a** Site-specific synthetic earthquake time-history at Bhuj, India; **b** comparison of response spectrum of the generated synthetic earthquake with that given in the IS 1893 (BIS 2016a); **c** wind velocity profile at top storey of the structure; **d** fast Fourier transform (FFT) of wind velocity at top storey of the structure; and **e** power spectral density (PSD) curve of wind velocity at top storey of the structure
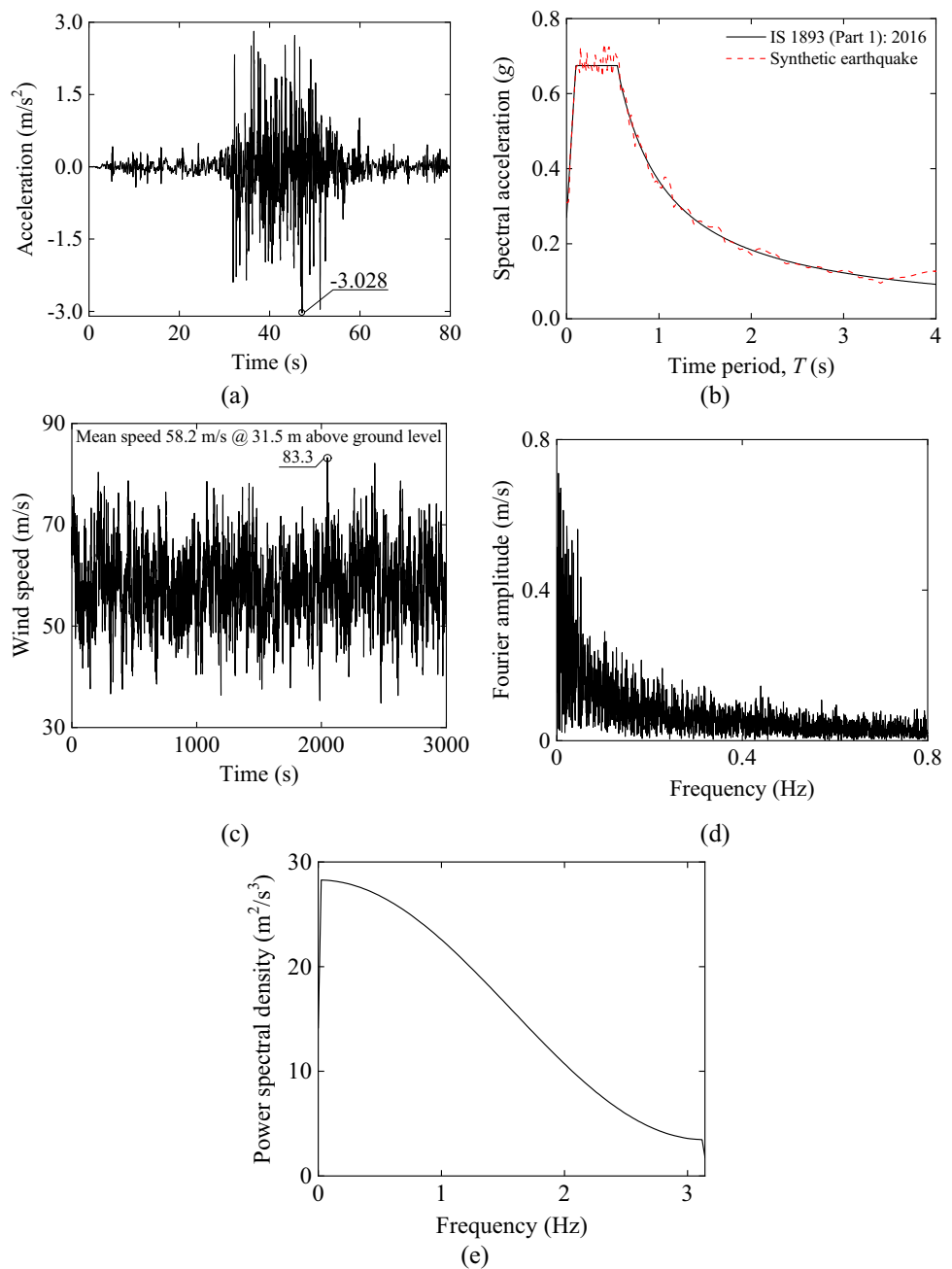
in the later years of construction. Note that delayed initiation of corrosion activity can be considered suitably in the analysis, once the instant of such initiation is known.

The probable damage in the structure at 100 years of its age is about 60% more than that is expected at its incipient stage, which is quite substantial, unless strengthening or retrofitting operations are undertaken. From the figure, it is observed that there is a marginal rise in the damage index value at 40 years of service-life as compared to its neighborhood region which can be attributed to increased structural response due to possible resonance of earthquake ground motion with one of the higher modes of the structure

as structure undergoes continuous change in its dynamic characteristics, i.e., stiffness reduction. This emphasizes the necessity of continuously monitoring the state of the structure so that such situations may be avoided during its service-life.

Wind Analysis of Structure

Wind force acting on a structure at a site or location is a function of wind velocity at that site followed by the gust factor. In the dynamic wind analysis, fluctuant component of wind speed is obtained from the peak gust velocity, $U_{3s\text{-}10}$

(3s-gust velocity at 10 m height from ground), which is defined in the design standards. To consider the effect of wind hazard on the structure considered here, site-specific dynamic wind velocity profile is obtained from NatHaz online wind simulator (NOWS): simulation of Gaussian multivariate wind fields (Kwon and Kareem 2006). This fluctuating wind velocity component is obtained using discrete frequency function with Cholesky decomposition and fast Fourier transform (FFT). From Eq. (20), the corresponding wind force acting on the structure can be determined as:

$$P = \frac{1}{2}\rho C_d A_b [U(t) + u(t)]^2, \tag{20}$$

where ρ is density of air; C_d is air drag coefficient; A_b is the bay area perpendicular to the wind velocity profile; $U(t)$ is the static or mean wind speed component; and $u(t)$ is the fluctuating wind velocity component. In the present study, 3 s-gust speed is considered as 75 m/s. The cut-off frequency is kept equal to the fundamental natural frequency of the structure under consideration, to obtain maximum possible response. The resultant average wind speed at the top floor is 58.2 m/s, and the maximum velocity component of the cyclonic wind time-history is 83.3 m/s as shown in Fig. 4c. This range of local cyclonic wind speed is in line with the India Meteorological Department (IMD) classification of cyclones in that region. Figures 4d and e show its frequency content and power spectral density (PSD) plots, respectively. Profiles of the wind forces are generated using a drag coefficient of 1.4 and they are then applied at each floor of the 9-storey building to conduct dynamic time-history analysis under wind excitation. The governing differential equation of motion, Eq. (21), for the 9-storey structure under wind excitation is written as:

$$M\ddot{x} + C\dot{x} + Kx = P, \tag{21}$$

where P is the wind load vector as defined in Eq. (20). Newmark's average acceleration scheme is used to determine the dynamic response of the structure under wind excitation through step-by-step integration approach. Peak top floor displacements over service-life of the structure under the action of wind-imparted forces are presented in Fig. 1d. These displacement values are used to determine resultant damage in the structure using the relation given in Eq. (17). Variation in the structural damage index for the cyclonic wind action during the service-life of the structure is presented in Fig. 3b. Similar to the earthquake excitation, uniform rise is observed in the structural damage with increasing age of the structure. However, damage in the medium-rise 9-storey RC structure under the action of local cyclonic wind action is quite less as compared to the medium intensity earthquake, similar to the observations made earlier by Roy and Matsagar (2020).

Service-Life Damage Analysis of Structures under Single and Multi-Hazard Scenarios

Effects of Earthquake and Chloride-Induced Corrosion

In the previous section, it has been shown that there is continuous increase in the structural damage when structural deterioration due to chloride-induced corrosion is considered, which might make the structure vulnerable under earthquake excitation. However, as observed from Fig. 3b, damage resulted in the structure due to earthquake alone is not so significant as to result in large inelastic deformation in any structural member although there is a definite decrease in the load-carrying capacity of the degraded structural members. The degradation in the load-carrying capacity of a member continues under the action of continuous chloride-induced corrosion of the steel reinforcement if no redressal on repair or restoration process in considered.

Let t_e represent the age of the structure at the time of incidence of the earthquake. Impact of earthquake-imposed damage on continuous corrosion-induced deterioration is presented in Fig. 5a. From Fig. 5a, it is evident that the structural damage which was limited to 0.28 (for $t_e = 20$ years) increased to 0.75 in the absence of structural repair or restoration during service-life of the structure, i.e., damage in the structure increased by approximately 150% over its service-life which might prove detrimental for the structure in future probable hazards. This is generally not incorporated in the initial design of the structure, which is used at the beginning of construction, and periodic maintenance and strengthening schedules are hardly ever related to this trend. Similar observation can be made for different earthquake scenarios, as shown in Fig. 5a. For checking the severity of the earthquake hazard, post-hazard behavior has been studied in terms of residual capacity-demand ratio or the factor of safety (FOS) for an interior column base. Design demand is the function of the dead and live loads that act on the structure. The load-carrying capacity of the structural members is a function of compressive strength of concrete, f_{ck} and rebar diameter as well as its strength, f_y which decreases over a period of time, as discussed in the preceding sections. The initial FOS of 3.67 markedly decreases to 1.35 (63% decrease) for an interior column base over the considered service-life of the structure for the scenario of earthquake ($t_e = 20$ years) including chloride-induced corrosion, as is presented in Fig. 6b. This underlines the fact that due consideration needs to be given to continuous structural degradation from various agents to determine post-hazard service-life of a structure and make an assessment if the desired FOS

Fig. 5 Service-life damage estimation in the RC structure for individual action of earthquake and cyclonic wind under continuous structural deterioration owing to chloride-induced corrosion (t_e and t_c denote the age of the structure at occurrence of earthquake and cyclone, respectively)

(a)   (b)
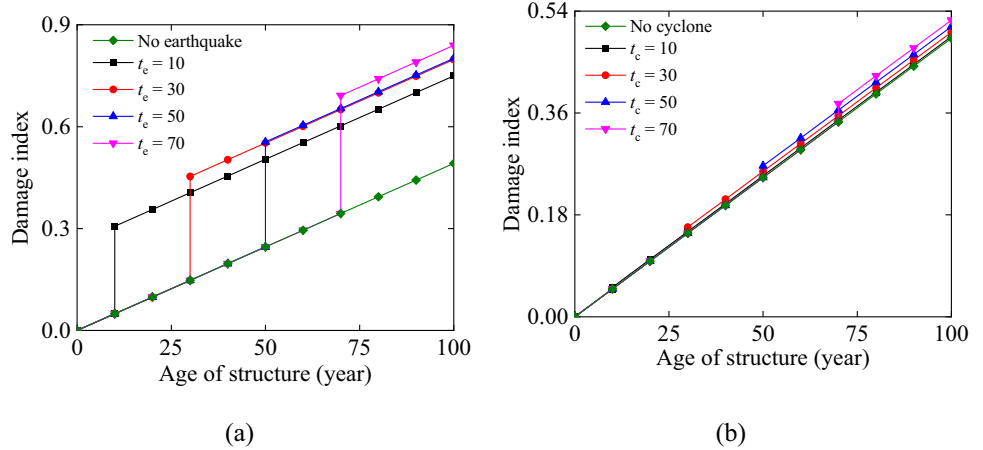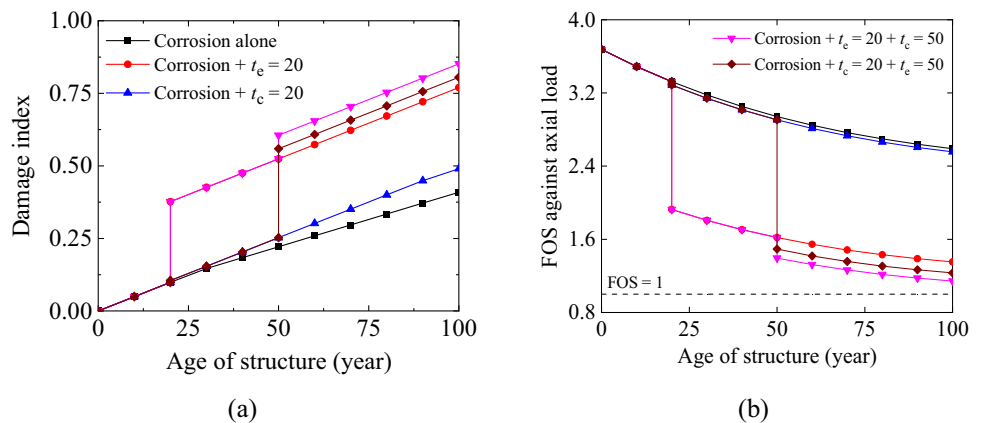
Fig. 6 Comparison of damage index and factor of safety (FOS) of an interior column base under permanent loads, when the structure is subjected to multi-hazard earthquake and wind excitation

(a)   (b)

is maintained over the service-life. If the effects of (a) repair and (b) restoration are considered as deliberated in section "Structural Deterioration due to Chloride-Induced Corrosion", the available FOS post-earthquake hazard for interior column base decreases respectively to (1) 1.67 and (2) 2.23 (nearly 55% and 40% decrease as compared to the initial FOS of 3.67), which indicates necessity to incorporate and model periodic structural maintenance so that the structure performs as intended even during its post-hazard service-life.

Effects of Wind and Chloride-Induced Corrosion

Since the damage incurred in the 9-storey building due to local cyclonic wind hazard is not significant as compared to that observed in the earthquake hazard, the effects of wind while accounting for the chloride-induced corrosion are approximately equivalent to that caused by the chloride-induced corrosion alone, as is presented in Fig. 5b. However, this behavior is limited to the site-specific conditions for the current structure with properties considered here and detailed study must be carried out for the structure under

consideration to avoid any non-proportionate behavior similar to that described in the previous section.

Multi-Hazard Effects of Earthquake and Wind on RC Structure

A parametric study has been carried out for studying the effects of the independent (uncorrelated) non-cascading earthquake and wind actions on the same structure, by varying the time of incidence of the two events, and by simultaneously considering the effects of corrosion-induced damages in the structure. The extent of structural damages is expressed in terms of a damage index, evaluated at the time of occurrence of the hazard, and are summarized in Tables 2 and 3. Age of the structure at the time of occurrence of the first hazard has been kept constant at 20 years, for earthquake as well as wind actions to obtain comparable results from the analysis, for the RC structure that hasn't experienced significant damage in the first 20 years. There could be several possible combinations, over the timespan, of occurrence of multiple hazards; however, the trend in the result would be similar, though damage values may not exactly be

Table 2 Cumulative damage index when the structure is first subjected to an earthquake at $t_e = 20$ year, and then by a cyclone at t_c (variable) later, while the structure is under continuous exposure to chloride-induced deterioration

t_c	Age of the structure (year)									
	10	20	30	40	50	60	70	80	90	100
30	0.049	0.377	0.479	0.528	0.578	0.627	0.676	0.725	0.774	0.824
40	0.049	0.377	0.426	0.545	0.594	0.643	0.692	0.742	0.791	0.840
50	0.049	0.377	0.426	0.475	0.606	0.655	0.704	0.753	0.802	0.852
60	0.049	0.377	0.426	0.475	0.524	0.673	0.722	0.771	0.820	0.869
70	0.049	0.377	0.426	0.475	0.524	0.573	0.749	0.798	0.847	0.896
80	0.049	0.377	0.426	0.475	0.524	0.573	0.623	0.807	0.856	0.905
90	0.049	0.377	0.426	0.475	0.524	0.573	0.623	0.672	0.891	0.940
100	0.049	0.377	0.426	0.475	0.524	0.573	0.623	0.672	0.721	1.001

Table 3 Cumulative damage index when the structure is first subjected to a cyclone at $t_c = 20$ year, and then by an earthquake at t_e (variable) later, while the structure is under continuous exposure to chloride-induced deterioration

t_e	Age of the structure (year)									
	10	20	30	40	50	60	70	80	90	100
30	0.049	0.105	0.459	0.508	0.557	0.606	0.655	0.705	0.754	0.803
40	0.049	0.105	0.154	0.522	0.571	0.620	0.669	0.719	0.768	0.817
50	0.049	0.105	0.154	0.203	0.559	0.608	0.658	0.707	0.756	0.805
60	0.049	0.105	0.154	0.203	0.252	0.631	0.680	0.730	0.779	0.828
70	0.049	0.105	0.154	0.203	0.252	0.302	0.715	0.764	0.813	0.862
80	0.049	0.105	0.154	0.203	0.252	0.302	0.351	0.771	0.821	0.870
90	0.049	0.105	0.154	0.203	0.252	0.302	0.351	0.400	0.854	0.903
100	0.049	0.105	0.154	0.203	0.252	0.302	0.351	0.400	0.449	0.931

the same. It is already stated that the effects of earthquake or cyclone on the structural response are pronounced when the deteriorating effects of corrosion in steel reinforcements are considered. A similar trend is observed in the multi-hazard analysis as well; however, structural degradation due to corrosion have more severe effects (around 1.5 times) on the multi-hazard analysis as that observed in case of the single-hazard analysis, which has been elaborated through Fig. 6a. Another interesting observation that can be made from Table 2 is, as the time gap between the occurrence of the first and second hazard increases, the overall damage induced in the structure is higher due to the increased deterioration on account of chloride-induced corrosion. As the hazard considered in the study are of medium to smaller level, the structure is not completely damaged ($D \geq 1$) in any case, except in the case when $t_e = 20$ and $t_c = 100$. In this specific case, the structure almost reaches ultimate performance point at 100 years of age, when hit by a cyclone (damage index increased from 72% to ~100%), causing a considerable inelastic deformation in the structural members. This emphasizes the need for a detailed multi-hazard analysis of an RC structure so that it remains safe against the worst multi-hazard combination even if the structure appears to be relatively safe with little expectation of inconsistent and unacceptable deformation. Similar inferences can also be drawn from Table 3 when cyclonic action on the structure is considered prior to the earthquake. By comparing results

reported in both Tables 2 and 3, it is observed that not only the magnitude of the hazard but also the order of occurrence of the same multiple hazard scenarios (at different times), and the time gap between the hazard occurrences are also significant factors in deciding the maximum probable service-life damage caused in the structure.

The results from the study evidently show that the occurrence of the earthquake (larger damage-producing event, in this case) prior to the wind hazard (lesser damage-producing event, in this case) causes severe damage to the structure as compared to the multi-hazard case in the reverse order. In the situations when the structure may seem reasonably less damaged; however, sudden occurrence of the second relatively lesser intense hazard may lead to large residual deformations in the structure (e.g., Table 2, $t_c = 100$ year case), thus resulting in a likely catastrophe.

For multi-hazard earthquake and cyclonic wind actions in terms of residual factor of safety (FOS), response of the structure is summarized in Tables 4 and 5. One case from each, Tables 4 and 5 is presented in Fig. 6b to showcase the nature of post-hazard strength in the structure. The case of (corrosion + $t_e = 20$ + $t_c = 50$) verifies the earlier observation of the larger overall impact on the structure when the structure is first hit by an earthquake (larger damage-producing event). The already damaged structure shows a significant fall in the FOS even at point of occurrence of the cyclone at $t_c = 50$ years. Any unprecedented

Table 4 Available factor of safety (FOS) of an interior column base when the structure is first subjected to an earthquake at $t_e = 20$ year, and then by a cyclone at t_c (variable) later, under continuous exposure to chloride-induced deterioration

Age of the structure (year)	t_c							
	30	40	50	60	70	80	90	100
0	3.677	3.677	3.677	3.677	3.677	3.677	3.677	3.677
10	3.489	3.489	3.489	3.489	3.489	3.489	3.489	3.489
20	1.926	1.926	1.926	1.926	1.926	1.926	1.926	1.926
30	1.651	1.806	1.806	1.806	1.806	1.806	1.806	1.806
40	1.553	1.508	1.705	1.705	1.705	1.705	1.705	1.705
50	1.469	1.425	1.394	1.619	1.619	1.619	1.619	1.619
60	1.398	1.354	1.323	1.278	1.545	1.545	1.545	1.545
70	1.337	1.294	1.264	1.219	1.153	1.483	1.483	1.483
80	1.287	1.245	1.215	1.171	1.105	1.085	1.431	1.431
90	1.246	1.204	1.175	1.131	1.066	1.046	0.965	1.388
100	1.213	1.171	1.142	1.099	1.035	1.014	–	0.804

Table 5 Available factor of safety (FOS) of an interior column base when the structure is first subjected to a cyclone at $t_c = 20$ year, and then by an earthquake at t_e (variable) later, under the continuous exposure to chloride-induced deterioration

Age of the structure (year)	t_e							
	30	40	50	60	70	80	90	100
0	3.677	3.677	3.677	3.677	3.677	3.677	3.677	3.677
10	3.489	3.489	3.489	3.489	3.489	3.489	3.489	3.489
20	3.286	3.286	3.286	3.286	3.286	3.286	3.286	3.286
30	1.684	3.141	3.141	3.141	3.141	3.141	3.141	3.141
40	1.583	1.531	3.015	3.015	3.015	3.015	3.015	3.015
50	1.498	1.445	1.492	2.906	2.906	2.906	2.906	2.906
60	1.426	1.374	1.418	1.337	2.812	2.812	2.812	2.812
70	1.366	1.314	1.357	1.275	1.158	2.731	2.731	2.731
80	1.315	1.265	1.307	1.226	1.108	1.086	2.663	2.663
90	1.274	1.224	1.266	1.186	1.069	1.045	0.941	2.605
100	1.240	1.191	1.232	1.153	1.038	1.014	–	0.830

loading on the structure after this instant can potentially cause many members of the structure to undergo large deformation as the structure enters in its inelastic zone and thereby mandating reconstruction of the structure on account of the damages being beyond repairable limits.

Effects of repair and restoration process, as deliberated in section "Structural Deterioration due to Chloride-Induced Corrosion", undertaken after the occurrence of a major damage-producing hazard, i.e., earthquake in the current study, are realized from Fig. 7a and b in which the resultant factor of safety (FOS) of base interior column against the action of permanent loads is presented for the two multi-hazard scenarios. For a multi-hazard case of earthquake ($t_e = 20$ year) and wind ($t_c = 50$ year) the damage index for the structure after the occurrence of cyclone is 0.082, in absence of repair and restoration process adopted. If the effects of repair actions are realized in the structure, this damage index reduced to 0.021, whereas if the effects of

restoration process are considered, the damage index further reduced to 0.011. Similar observations can be made in terms of factor of safety (FOS) at the end of design service-life of the structure. In absence of any repair and restoration process, the FOS of base interior column reduces from 3.67 to 1.14 (i.e., 69% reduction). If the effects of repair and restoration processes are considered, this FOS reduces to 1.63 and 2.21 (i.e., 55% and 40% reductions), respectively from 3.67. Similar observations are made in the multi-hazard case where cyclonic wind action precedes the earthquake hazard ($t_c = 20$ year and $t_e = 50$ year). Different cases considered and studied in this context demonstrate the importance of the structural repair and restoration activities undertaken even when the structure seems to be less damaged relatively, as another hazard at any time can potentially trigger an unanticipated behavior of the RC structure which may lead to impending loss of life and property, as was observed during several natural hazards in the past.

Fig. 7 Comparison of factor of safety (FOS) of an inner column base under permanent loads, when the structure is subjected to multi-hazards earthquake and wind excitation while considering the effects of structural repair and restoration, undertaken after the occurrence of earthquake
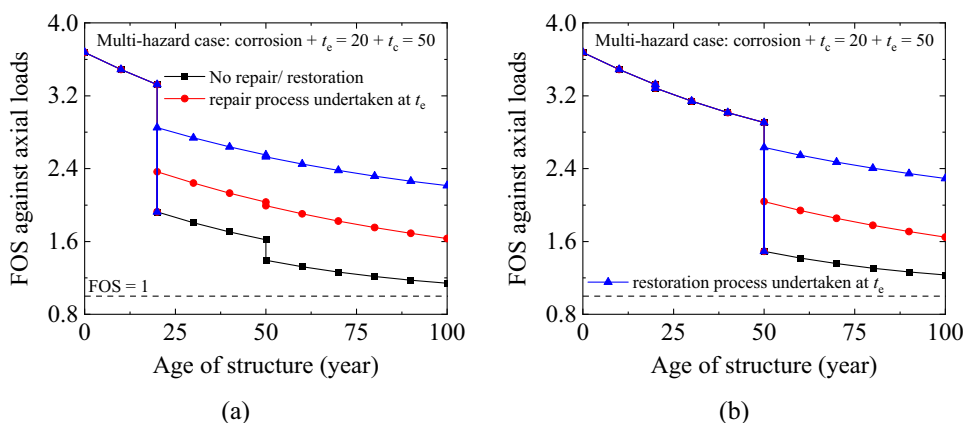
Conclusions

Service-life multi-hazard earthquake and wind analyses of a 9-storey reinforced concrete (RC) building is conducted in the present study. The structure is subjected to earthquake time-history compatible to the response spectrum given in the Indian standard, IS 1893 (BIS 2016a) corresponding to moderate intensity; and, a site-specific cyclonic wind load condition while undergoing continuous structural deterioration due to chloride-induced corrosion in all structural members during the service-life. Response of the structure is recorded in terms of a damage index and residual factor of safety in a column base against the action of permanent loads, i.e., dead and live loads. Based on the numerical results obtained and reported here the following conclusions are drawn:

1. Continuous structural deterioration caused due to environmental agents such as chloride ions, depending on the location of a structure near saline environment/ waterbody, may be significant, even in the structures which are designed as per the code guidelines, as much to increase the structural damage by 60% due to the major extreme events following, such as earthquake and cyclonic wind. Therefore, the causal effects of such service-life degradation phenomena cannot be neglected while performing holistic analysis of the structure from such hazards that it may experience over its design (service) life.

2. The possibility of experiencing failure in the structure increases when it is under the action of multiple hazards of minor or medium intensity, such as earthquake and wind, though it is designed for the extreme load cases in either of the two combinations independently. Such instances are plausible because the medium level hazards are more probable as compared to the occurrence of extreme hazards, and minor structural damages caused by them often go unnoticed. However, when their cumulative effect is considered over the period of service-life of a structure, the resultant damage is several folds increased than what is expected under their singular action. This mandates the structural designers conducting service-life multi-hazard analysis and design of civil infrastructures.

3. Timely structural repair or restoration actions has been found to not only reduce the risk (threat) of structural damage by a significant margin (approximately 75%) but also slow down the continuous structural deterioration due to various environmental actions, e.g., corrosion of steel in the RC members. Thus, predetermined scheduled maintenance of an RC structure is recommended so as to retain the desired factor of safety (FOS) during the design (service) life. Carrying out service-life evaluation of the FOS is therefore essential at the design stage itself.

References

Aly AM, Abburu S (2015) On the design of high-rise buildings for multihazard: fundamental differences between wind and earthquake demand. Shock Vibr 2015:148681

Avramidis I, Athanatopoulou A, Morfidis K, Sextos A, Giaralis A (2016) Fundamental principles for the design of earthquake-resistant structures, Eurocode-compliant seismic analysis and design of R/C buildings, vol 38, pp 1–57. Springer, Cham, Switzerland

Basheer PAM, Chidiac SE, Long AE (1996) Predictive models for deterioration of concrete structures. Constr Build Mater 10(1):27–37

BIS (1987a) IS 875: code of practice design loads (other than earthquake) for buildings and structures part 1: dead loads—unit weights of building materials and stored materials, Bureau of Indian Standards (BIS), New Delhi, India

BIS (1987b) IS 875: code of practice design loads (other than earthquake) for buildings and structures part 2: imposed loads, Bureau of Indian Standards (BIS), New Delhi, India

BIS (2000) IS 456: plain and reinforced concrete—code of practice, Bureau of Indian Standards (BIS), New Delhi, India

BIS (2009) IS 13935: seismic evaluation, repair and strengthening of masonry buildings—guidelines, Bureau of Indian Standards (BIS), New Delhi, India

BIS (2015) IS 875: design loads (other than Earthquake) for buildings and structures—code of practice part 3: wind loads, Bureau of Indian Standards (BIS), New Delhi, India

BIS (2016a) IS 1893: criteria for earthquake resistant design of structures part 1: general provisions and buildings, Bureau of Indian Standards (BIS), New Delhi, India

BIS (2016b) National Building Code of India, Bureau of Indian Standards (BIS), New Delhi, India

Cao VV, Ronagh HR, Ashraf M, Baji H (2014) A new damage index for reinforced concrete structures. Earthquake Struct 6(6):581–609

Chen D, Mahadevan S (2008) Chloride-induced reinforcement corrosion and concrete cracking simulation. Cement Concr Compos 30(3):227–238

Chen YM, Fan KS, Chen LC (2010) Requirements and functional analysis of a multi-hazard disaster-risk analysis system. Hum Ecol Risk Assess Int J 16(2):413–428

Chopra AK (2016) Dynamics of structures: theory and applications to earthquake engineering, 5th edn. Pearson Education, India

Chulahwat A, Mahmoud H (2017) A combinatorial optimization approach for multi-hazard design of building systems with suspended floor slabs under wind and seismic hazards. Eng Struct 137:268–284

Coronelli D, Gambarova P (2004) Structural assessment of corroded reinforced concrete beams: modeling guidelines. J Struct Eng 130(8):1214–1224

Cui Z, Alipour A, Shafei B (2019) Structural performance of deteriorating reinforced concrete columns under multiple earthquake events. Eng Struct 191:460–468

Duthinh D, Simiu E (2010) Safety of structures in strong winds and earthquakes: multihazard considerations. J Struct Eng 136(3):330–333

FEMA 356 (2000) Prestandard and commentary for the seismic rehabilitation of buildings, Federal Emergency Management Agency (FEMA), American Society of Civil Engineers (ASCE), USA

Ferreira F, Moutinho C, Cunha Á, Caetano E (2020) An artificial accelerogram generator code written in MATLAB. Eng Rep 2(3):1–17

Gardoni P, LaFave JM (2016) Multi-hazard approaches to civil infrastructure engineering. Springer International Publishing AG, Cham, Switzerland

Hait P, Sil A, Choudhury S (2019) Overview of damage assessment of structures. Curr Sci 117(1):64–70

Kameshwar S, Padgett JE (2014) Multi-hazard risk assessment of highway bridges subjected to earthquake and hurricane hazards. Eng Struct 78:154–166

Kappos AJ (1997) Seismic damage indices for RC buildings. Prog Struct Mat Eng 1(1):78–87

Kwon D, Kareem A (2006) NatHaz online wind simulator (NOWS): simulation of Gaussian multivariate wind fields, NatHaz Modeling Laboratory Report, University of Notre Dame, USA, http://windsim.ce.nd.edu. Accessed 9 Jan 2022

Lemaitre J (1984) How to use damage mechanics. Nucl Eng Des 80(2):233–245

Li Y, van de Lindt JW (2012) Loss-based formulation for multiple hazards with application to residential buildings. Eng Struct 38:123–133

Molina FJ, Alonso C, Andrade C (1993) Cover cracking as a function of rebar corrosion: part 2—numerical model. Mater Struct 26:532–548

Newmark NM (1959) A method of computation for structural dynamics. J Eng Mech Div Am Soc Civ Engineers (ASCE) 85(3):67–94

Nikellis A, Sett K, Whittaker AS (2019) Multihazard design and cost-benefit analysis of buildings with special moment-resisting steel frames. J Struct Eng 145(5):4019031

Noguchi T, Nemati KM (2007) Relationship between compressive strength and modulus of elasticity of high-strength concrete. In: Proceedings of the 6th international conference on fracture mechanics of concrete and concrete structures, Taylor and Francis, London, UK, pp 1305–1312

Otieno M, Beushausen H, Alexander M (2016a) Chloride-induced corrosion of steel in cracked concrete—Part I: experimental studies under accelerated and natural marine environments. Cem Concr Res 79:373–385

Otieno M, Beushausen H, Alexander M (2016b) Chloride-induced corrosion of steel in cracked concrete—part II: corrosion rate prediction models. Cem Concr Res 79:386–394

Pack SW, Jung MS, Song HW, Kim SH, Ann KY (2010) Prediction of time dependent chloride transport in concrete structures exposed to a marine environment. Cem Concr Res 40(2):302–312

Park YJ, Ang AHS, Wen YK (1985) Seismic damage analysis of reinforced concrete buildings. J Struct Eng 111(4):740–757

Roy T, Matsagar V (2019) Effectiveness of passive response control devices in buildings under earthquake and wind during design life. Struct Infrastruct Eng 15(2):252–268

Roy T, Matsagar V (2020) Probabilistic assessment of steel buildings installed with passive control devices under multi-hazard scenario of earthquake and wind. Struct Saf 85:101955

Roy T, Matsagar V (2021a) Multi-hazard analysis and design of structures: status and research trends. Struct Infrastruct Eng. https://doi.org/10.1080/15732479.2021.1987481

Roy T, Matsagar V (2021b) Multi-hazard analysis and design guidelines: recommendations for structure and infrastructure systems in the Indian context. Curr Sci 121(1):44–55

Sinha R, Shiradhonkar SR (2012) Seismic damage index for classification of structural damage—closing the loop. In: Proceedings of the 15th world conference on earthquake engineering, Libosa, Portugal

Tofeti-Lima T, Ann KY (2020) Efficiency of different electrolytes on electrochemical chloride extraction to recover concrete structures under chloride-induced corrosion. Adv Mater Sci Eng 2020:5

Vecchio FJ, Collins MP (1986) Modified compression-field theory for reinforced concrete elements subjected to shear. ACI J Am Concrete Inst (ACI) 83(2):219–231

Venanzi I, Lavan O, Ierimonti L, Fabrizi S (2018) Multi-hazard loss analysis of tall buildings under wind and seismic loads. Struct Infrastruct Eng 14(10):1295–1311

Wang Z, Martinez-Vazquez P, Zhao B (2020) Pushover analysis of structures subjected to combined actions of earthquake and wind. Eng Struct 221:111034

Wu YF, Yun Y, Wei Y, Zhou Y (2014) Effect of predamage on the stress-strain relationship of confined concrete under monotonic loading. J Struct Eng 140(12):04014093

Zameeruddin M, Sangle KK (2016) Review on recent developments in the performance-based seismic design of reinforced concrete structures. Structures 6:119–133

Zhou Y, Gencturk B, Willam K, Attar A (2015) Carbonation-induced and chloride-induced corrosion in reinforced concrete structures. J Mater Civ Eng 27(9):04014245